Shear zone liquefaction in mass transport deposit emplacement: A multi-scale integration of seismic reflection and outcrop data

Published version:

DOI:10.1016/j.margeo.2014.05.001

(Article begins on next page)

Marine geology 4/2014, http://dx.doi.org/10.1016/j.margeo.2014.05-001

Shear zone liquefaction in mass transport deposit emplacement: A multi-scale integration of seismic reflection and outcrop data

Ogata, K. [1,5], Mountjoy, J.J. [2], Pini, G.A. [3], Festa, A. [4] and Tinterri, R.[5]

[1] Department of Arctic Geology, University Centre in Svalbard, P.O. Box 156, 9171, Longyearbyen, Norway (kei.ogata@gmail.com)

[2] National Institute of Water and Atmospheric Research, Private Bag 14901, Wellington, New Zealand (joshu.mountjoy@niwa.co.nz)

[3] Università degli Studi di Trieste, Dipartimento di Matematica e Geoscienze, 34128 Trieste, Italy (gpini@units.it)

[4] Dipartimento di Scienze della Terra, Università di Torino, 10125 Torino, Italy (andrea.festa@unito.it)

[5] Dipartimento di Fisica e Scienze della Terra "Macedonio Melloni", Università degli Studi di Parma, Campus Universitario - Parco Area delle Scienze 157/A, I-43124 Parma, Italy (roberto.tinterri@unipr.it)

Abstract

We present the integrated outcrop-geophysical study of two mass transport complexes, the exhumed Specchio unit in the Northern Apennines of Italy and the Holocene Poverty unit in the Hikurangi margin of New Zealand. The combination of micro- to meso-scale structural, stratigraphic and sedimentologic analyses carried on continuous three-dimensional outcrops, with large-scale structural and morphologic data deriving from seismic/acoustic imaging of the present-day continental margins, allow important considerations on submarine landslide processes and mechanisms through the broader (up-scaled and down-scaled) understanding of the mass transport-related structural associations. We compare the discontinuous high-amplitude, reverse-polarity reflectors observed within the Poverty with the syn-sedimentary, ductile shear zones found within the Specchio mass transport complex. The seismic signature of such structures suggests localized fluid overpressure along detachment/thrust zones due to shearing and loading of undrained, water-saturated, fine-grained material, developed along with the slide mass movement. The outcrop expression of these structures is tentatively attributed to m- to tens of m-thick shear zones comprising large amounts of sedimentary matrix which separate and accommodate the differential movements of the internal slide components (e.g. slide blocks, olistoliths). The sedimentary matrix is an unsorted, lithologically mixed medium characterized by a scale-invariant "block-in-matrix" fabric (i.e. brecciated, mud-supported), that injects, sustain and surrounds discrete slide elements (from particles to blocks) and interpreted as a hyper-concentrated (liquefied/fluidized) suspension of water and scattered sediments developed in fluid overpressure

conditions. We highlight the fundamental role of shearing-related liquefaction as one of the main factors controlling slide mobility through the "lubrication" of the internal and basal friction forces. The analysis of such features can therefore provide important information for the characterization of mass transport deposits developed from potentially catastrophic, long run-out mass transport events, and consequently, to better understand their possible socio-economic impact in terms of tsunamigenic potential.

Keywords: exhumed mass transport complexes; sedimentary matrix; ductile shear zones; liquefaction; fluid overpressure

1. Introduction

The recent achievements in marine geology on seafloor and sub-seafloor mapping allow important consideration on recent to modern submarine landslides, giving general clues on their overall morphology and areal extent (Canals *et al*., 2004; Frey-Martinez *et al*., 2006; Gee *et al*., 2007; Bull *et al*., 2009). One of the main challenges arising from these studies revolves around the characterization of the complex internal anatomy of such deposits, and thus, the correct understanding of the genetic mechanisms and processes, which is crucial for offshore hydrocarbon exploration, and geohazard assessment and mitigation (see Hampton *et al.*, 1996; Mosher *et al.*, 2009; Kawamura *et al.*, 2012).

Most of the internal structures of a slide body are developed at the meso-scale (meters to ten of meters), and therefore hardly recognizable through geophysical methods being well below the standard seismic resolution. Moreover, the high internal heterogeneities and the combined occurrence of materials with different degrees of consolidation contribute to complicate the seismic signal, resulting in acoustic artifacts and transparent zones. On the other hand, at the outcrop scale, these internal structures can be observed and described in detail (Lucente and Pini, 2003; Callot *et al.*, 2008a; 200b; Ogata *et al.*, 2012a), and, depending on the quality and the continuity of the exposures, such analyses could be up-scaled to fit to the seismic field of observation. In this framework we believe that a systematic comparison with fossil mass transport deposits cropping out in orogenic belts (i.e. sedimentary mélanges) would strongly contribute in solving these problems (Festa *et al.*, 2010a, 2010b, 2012). Currently, apart from the general and useful review of the mass transport deposits' seismic-scale structures provided by Bull *et al.* (2009) and the preliminary (and generally conceptual) attempt of comparison between seismic and outcrop data recently proposed by Bull and Cartwright (2010), there is still a general lack of works using an integrated approach in the study of submarine landslides. This leads to a gap in the basic knowledge of the meso-scale internal processes and related structures, and their relationship with larger scale features.

We present an attempt to combine and integrate geophysical and outcrop data in order to establish a continuity of observation at different scales, crucial for the study of vertically- and laterally-extensive submarine landslide deposits. Whereas the standard subsurface and seafloor imagery technology provides the gross morphology, areal extension and internal organization of a mass transport deposit, often providing a complete picture of a mass transport complex, the highest resolution of multi-channel seismic reflection data required to image such features is ca. 5 m or coarser. On the other hand, outcrop studies allow multi-scale analyses (depending on the exposure conditions), providing resolution from the microscopic scale up to the cartographic scale (comparable with the geophysical scale). Through the study of comparable onland and offshore analogues it is virtually possible to fill the mutual gaps of the two different approaches, allowing the construction of a more comprehensive and better-constrained framework.

The aim of this work is to address these issues providing a detailed integration of structural data coming from geophysical and outcrop examples characterized by comparable scales and depositional settings. We present a compilation of outcrop data coming from the Specchio mass transport complex, belonging to the Eocene-Oligocene intra-slope basin succession (*i.e.* Epiligurian Units) developed atop the exhumed Ligurian accretionary wedge in the Northern Apennines in Italy (Ogata *et al.*, 2012a, 2012b). These field-based observations are tentatively up-scaled and compared to the Holocene Poverty mass transport complex of the Hikurangi margin in New Zealand (Mountjoy and Micallef, 2012).

2. Geological background and case studies overview

Our data come from two examples of large submarine mass failures emplaced in subduction/collision-related wedge top depositional settings and characterized by comparable physiographic and depositional contexts. The Specchio mass transport complex is an ancient, exhumed example from the Northern Apennines of Italy, while the Poverty mass transport complex comprises Holocene slide deposits emplaced in an active subduction system off the East Coast of New Zealand (fig. 1). These two examples are well suited for comparison as they are of a similar scale (both in terms of areal extension and thickness), depositional setting (i.e. intra-slope, wedge-top) and overall internal architecture (i.e. stacking/amalgamation of more events). These general common features are summarized in the table of fig. 1C.

2.1 The Specchio mass transport complex

The upper Priabonian-lower Rupelian Ranzano Unit of the Epiligurian succession of the Northern Apennines represents a perfect example of syn-orogenic, siliciclastic infilling of an intra-slope, wedge-top mini-basin (i.e. small-scale) system characterized by depocenters about 5-10 km in size. These structurally confined basins were located atop the deforming Ligurian oceanic accretionary prism during its tectonic transport toward the eastern sectors, following the complex continental convergence between African (Adria) and European plates, in a time interval comprised between the latest stages of the Alpine orogenesis and the inflection (i.e. flexural down-bending) of the Apenninic foreland (Castellarin, 1994; Mutti *et al.*, 1995; Martelli *et al.*, 1998; Cavazza *et al.*, 2004; Marroni *et al.*, 2010).

The analyzed Specchio unit is a mass transport complex hosted in the middle-basal part of the Ranzano Sandstone stratigraphic succession (Martelli *et al.* 1998), which is mainly constituted by proximal, coarse-grained, low efficiency (*sensu* Mutti, 1992) turbidite deposits accumulated in relatively deep water setting (middle-upper bathyal depth; Di Giulio et al., 2002). This mass transport complex is characterized by an estimated areal extent conservatively calculated around ~ 1.500 km^2 and an average thickness of ~ 100 m, and it is generated by the rapid, polyphased accumulation of at least three mass transport deposits characterized by different paleo-transport directions: 1) a basal one(s), coming from the southern sectors, of mixed extra- and intrabasinal composition, originated from shallow-tectonic positive structures (e.g. anticline culminations) and other topographic highs close to the depocentral areas, 2) a middle one, coming from the northern sectors, of mainly intrabasinal composition, originated from structural highs located in a relatively distal position from the main depocenters, and 3) an upper one(s) coming from northern sectors, composed of shallow-water related sediments failed from the basin margins, in proximal position with respect to the inferred feeding areas (*i.e.* coastal areas) (fig. 2). In this framework, the Specchio unit is thought to represent the rapid sedimentary response to a general rearrangement of the source-depositional system, operated by the synergic effect of an active syn-sedimentary tectonism and sea level changes, possibly acting together from the Early Oligocene (Ogata *et al.*, 2012b).

In terms of sedimentary processes, each individual depositional event comprises a bipartite flow made up by a lower matrix-dominated and an upper block-dominated parts (Ogata *et al.*, 2012a; 2012b) which in turn correspond to debris flows and blocky flows, respectively (in the sense of Mutti *et al.*, 2006). The local occurrence of slump-type deformations (i.e. coherent slide movement achieved through syn-sedimentary shear zones; see Ogata *et al.*, 2012a) is restricted to the sand-dominated substrate and the internally folded oversized blocks. The matrix composition and amalgamation, and the various expressions of post-emplacement fluid escape and depressurization acting together, suggest that the Specchio mass transport deposits are composed by (i) a cohesive upper part (i.e. block-dominated portion), behaving as a relatively coherent sheet of separated, passively-transported rafts ("rigid plug" of Middleton and Hampton, 1973), and (ii) a non-cohesive, lower part (i.e. matrix-dominated portion) behaving as a non-Newtonian fluid (hyperconcentrated suspension in the sense of Mutti, 1992). In this framework, the matrix itself is thought to support internal slide elements (from mm-sized clasts to m-sized blocks) due to its yield strength, whereas at larger scale, the matrix-dominated portion is inferred to sustain the entire flow through the upward and dispersive forces of the fluid excess pressure, reducing the basal/internal frictions and enhancing the slide mobility (Ogata *et al.*, 2012a; 2012b; Pini *et al.*, 2012). The same mechanisms have been also hypothesized for some modern, long run-out submarine landslides (Mulder and Alexander, 2001).

2.2 The Poverty mass transport complex

The modern mass transport complex discussed in this paper occurs on the upper slope of the Hikurangi Margin, an active subduction margin off the East Coast of New Zealand (fig. 3) (Barnes *et al.*, 2010; Lewis and Pettinga, 1993).

The Poverty mass transport complex, also referred to as the Poverty Debris Avalanche in literature, is the result of slope modification within the Poverty re-entrant (Mountjoy and Micallef, 2012). The Poverty re-entrant is a margin-scale morpho-tectonic feature interpreted to be the result of seamount impacts from the incoming Pacific Plate, initiating approximately 1 Ma ago (Pedley *et al.*, 2010). The structural and sedimentary post-impact reconfiguration of the margin is achieved by the development of submarine canyon and slope-gully systems, as well as large-scale mass failures (Orpin, 2004; Walsh *et al.*, 2007; Mountjoy *et al.*, 2009; Pedley *et al.*, 2010). In this area, Quaternary sedimentation developed thick shelf-basin sequences and shelf-edge clinoforms, unconformably overlying, with draping and onlapping relationships, Cretaceous to Miocene rocks, which are exposed in the gullies and canyon heads of the Poverty re-entrant headwall (Mountjoy and Barnes, 2011).

The Poverty mass transport complex is one of the largest (~250 km^2) blocky debris deposits of the Hikurangi margin, and covers most of the gently inclined (ca. 1°) seafloor of the Paritu basin between 1100 and 1500 m water depth. The deposit is sourced from a restricted head area (34-46 km^3) below the shelf break (900-1150 m water depth) and has likely failed in multiple (2-4), retrogressive depositional events (Mountjoy and Micallef, 2012; Pouderoux *et al.*, 2012). Seismic reflection data indicate complex internal deformation that is the topic of this study.

3. Methods and data

3.1 The Specchio mass transport complex

The Specchio mass transport complex has been primarily investigated through a detailed field mapping (1:5.000 scale) to detail the overall internal and external characteristics of the component mass transport deposits, their vertical and lateral changes, relationships with the host sedimentary succession and general tectonic-stratigraphic context.

High-resolution analyses and observations have been performed within the different unit at various locations and stratigraphic levels in order to identify the different mass transport facies (Ogata, 2012a; 2012b): meso- to micro-scale structural and sedimentologic analyses have been performed to represent the spatial/geometric distribution of the internal elements, their provenance and to highlight their bulk deformation mechanism. Detailed stratigraphic logging (1:50 scale) of the over- and underlying bedded successions has been performed to constrain the position of the investigated unit within the sedimentary column and reconstruct the syn- to post-depositional physiographic variations related to the slide emplacement. Complementary micro-structural and sedimentologic analyses (i.e. transmitted light optical microscopy) have been performed on thin sections coming from the sedimentary matrix of the component mass transport deposits.

To clarify the used terminology, we here define as “ductile-like” the structures showing mesoscale to microscale continuous deformation caused by independent (i.e. intergranular) particulate flow occurred without appreciable mechanical grain breakage (cataclasis, Knipe, 1986) within non-consolidated sediments with the effective stress strongly reduced by fluid overpressure (mesoscopic ductile behavior;

Pini, 1999). By analogy, these structures (sometimes resembling metamorphic ductile zones of concentrated deformation, such as the classical mylonites), are classified with the standard terms (Passchier and Trouw, 2005) with the addiction of the suffix "pseudo-" to stress their non-tectonic origin and the absence of any kind of intra-crystalline plasticity, and used as kinematic indicators to solve the shearing sense of the associated structures.

Since the identification of the source areas and the run-out paths is not obvious in outcrop studies, we used a combination of the standard methods proposed in the literature to unravel the local and general paleo-transport directions (Bradley and Hanson, 1998; Lucente and Pini, 2003; Strachan and Alsop, 2006), collecting and analyzing standard meso-structural data on plastic, soft-sediment deformation structures and structural associations such as 1) non-cylindrical and asymmetrical folds (i.e. vergences, axes, axial planes, plunges, sheath-fold main axes, etc.), and 2) low-angle syn-sedimentary faults and shear zones (i.e. shear planes, lineations, long axes of elongated elements, axes of associated drag folds, etc.), observed within the matrix- and block-dominated parts of the component mass transport deposits bodies.

3.2 The Poverty mass transport complex

The Poverty mass transport complex has been imaged with a combination of multibeam bathymetric data and multi-channel seismic reflection data. Multibeam data on the continental slope are gridded at 25 m and are from Simrad EM300 and EM302 surveys carried out between 2001 and 2011 (Mountjoy and Micallef, 2012; Pedley *et al.*, 2010). Shelf/upper slope data, gridded at 10 m, include Simrad EM 3000 and Atlas Hydrosweep MD-2/30 (Royal New Zealand Navy) data. High-resolution data are augmented with a regional 100 m bathymetric grid built from a combination of 12 kHz SIMRAD EM12 Dual multibeam and single beam echo sounder bathymetric data held in the NIWA database. Three multichannel seismic reflection (MCS) datasets are presented in this study: 1) 6-fold, 24-channel seismic profiles acquired with a GI-gun source in 45/105 mode in 2001, 2) up to 960-channel high fold 2D seismic reflection data recorded to 12 seconds TWT in 2005, and 3) 12-fold, 48-channel seismic profiles acquired with a twin GI-gun source in 45/105 mode in 2011 (Barker *et al.*, 2009; Mountjoy and Barnes, 2011; Pedley *et al.*, 2010). An assumed sediment velocity of 1.800 m/s has been used for volume calculations and time-depth conversion.

4. Results

4.1. The Specchio mass transport complex

Ductile-like, syn-sedimentary shear-zones are commonly expressed by low-angle thrust and subordinately normal faults, sometimes and locally steep-dipping, affecting both matrix and blocks but with different characteristics. Such shear zones are represented by discrete intervals, centimeters- to several meters-thick and meters- to tens of meters-long, characterized by a contrasting texture with the surrounding lithologies. These structures do not show discrete shear surfaces or planes, being instead represented by intervals of remolded and mixed appearance, due to the internal occurrence of elongated bands and lenses of sedimentary matrix, comprising different types of pseudo-ductile shearing clues: 1) pseudo-SC (i.e. Shear/Cleavage) structures, 2) pseudo-Sigma structures, 3) hydroplastic, intrafolial folds, 4) iso-orientation of rigid oblate clasts, 5) preferential elongation of plastic intra-clasts, 6) disaggregation/deformation bands and 7) rheomorphic-like, fluidal structures (fig. 4).

Depending on the composition and consolidation degree of the involved materials, these shear zones are usually characterized by a local enhancement in the concentration of matrix, developed through frictional deformation and disaggregation of the involved sediments. The internally banded pattern, defined by isoclinally folded and elongated mud intraclasts and particle alignments, is generally coherent with the associated shear plane testifying shearing in overall visco-plastic conditions (fig. 5).

The basal shear zone is usually thicker and more laterally continuous than the internal ones and it is also typically characterized by the occurrence of higher amount of intrabasinal, liquefied material belonging to the substrate. Secondary internal shear zones mainly develop along the boundaries of discrete slide elements (*i.e.* blocks, un-dissociated masses), comprising a relatively small amount of matrix arranged in discontinuous pinching-and swelling seams and lenses. Sometimes such shear zones are rooted into the basal shear interval, suggesting that the same liquefied material of the basal shear zone has been injected upward (fig. 6).

Microstructural observations performed on thin sections reveal no evidence of tectonic-related brittle deformations (*e.g.* cataclasis, syn-kinematic mineralized veins or fractures, stylolites) within such structures. Microinjections of matrix into preexisting discontinuities and voids affecting the single grains (0.5 mm scale), pseudo deformation/disaggregation bands, iso-orientation of elongated particles and fluidal structures suggest shearing under low confining stress and generalized fluid overpressure conditions (fig. 7). These observations are supported by the results of experimental and numerical modeling, as summarized in Goren *et al.*, (2010) and Goren *et al.* (2011).

Combining the structural data from the shear zones, tuned with the above-mentioned kinematic indicators used to define the general shearing sense, with the spatial distribution of asymmetric folds (i.e. separation-arc, mean-axis and sheath-fold long axis methods; Bradley and Hanson, 1998; Lucente and Pini, 2003; Alsop and Holdsworth, 2004; Strachan and Alsop, 2006), and the arrangement of the internal element imbrication (Ogata *et al.*, 2012a, 2012b), an overall down-slope transport direction has been estimated for each component mass transport deposits. The general vergence and the stacking relationships of these shear zones, mostly represented by low-angle thrusts arranged in splays and imbricated sets, provide additional kinematic information to understand their mechanism and mode of emplacement.

Structural associations typically align parallel to the inferred position of the lateral boundaries of the slide mass (i.e. slide margins/levees). Detailed observations on three-dimensional outcrops, integrated with the estimation of paleo-transport directions, highlight a strong lateral anisotropy/heterogeneity of the internal meso-scale structural arrangement, either in cross and longitudinal view. In cross section (i.e. looking parallel to the slide movement), this is evident from the common occurrence of low-angle shear zones and structural associations (e.g. pop up- and flower structures, double-vergent box folds, sheath folds, folds' interference patterns) characterized by non-concordant to opposite shearing and verging sense recording an overall lateral buckling transversally to the mean transport direction, whereas in long section (i.e. looking laterally to the slide movement) they appear to record an overall preferential down-slope direction (fig. 8).

4.2 The Poverty mass transport complex

The internal structure of the Poverty mass transport complex is revealed in multi-channel seismic reflection data (MCS). Mass transport deposits are identified by discontinuous weak reflectivity compared to the overall coherent reflectivity of the host sediments (e.g. Lamarche *et al.*, 2008).

In multibeam data the upper surface of the Poverty mass transport complex is irregular and it shows a blocky roughness characterized by marked lateral changes. The uneven surface of the deposit is given by the presence of individual rafted slide blocks varying from ca. 1000 m across in the up-slope part to less than 100-150 m in the down-slope part, defining two different portions of the slide mass characterized by different geometry and roughness characteristics (figs. 3C). In cross section, these slide blocks appear as localized zones with internally coherent and continuous reflectors, sometimes deformed but usually pseudo-concordant with the basal surface, surrounded by a background of discontinuous reflectors and transparent zones (see figs. 3D and 9E).

Down with the length of the landslide body we recognize distinctive longitudinal transformations in the structural style. Within the upper portion of the body, thrusts and folds, indicating a compressional regime, dominate the structural style. Further down the length of the slide mass, structures become more subdued and dominated by normal faulting, indicating down-slope tensions within the debris body. These structures show curved to roughly rectilinear axes, mostly disposed perpendicular to the inferred slide movement and becoming progressively parallel to it toward the slide margins, following the overall lobate-like shape of the slide body.

In the down-slope portion, the deposit indicates compressional deformation in multiple locations, as suggested by the occurrence of tens of meters-sized thrust faults defined by hanging wall and footwall cutoffs. In places it is apparent that internal units have been thrust over one another (figs. 9B and 9C).

Remarkably, the above described thrust faults are in many cases accompanied by high amplitude reflectors bounding the surface that define the basal *décollement*. These internal discontinuous reflectors are commonly defined by inverse polarity, indicating discrete low-density contrast zones (figs. 9D and 9E). As recognized elsewhere in seismic reflection data (e.g. Bull *et al.*, 2009; Yamada *et al.*, 2012) the basal slide horizon is a distinct unit of lower acoustic impedance compared to the coherent high amplitude underlying reflectors below (defining non-mass transport sedimentation), which may be extensively deformed or completely scoured by the overlying material (Vardy *et al.*, 2012). Accordingly, the semi-continuous, coherent reflectors found within the slide body are interpreted to separate (at least 2) different deposits from the same general source area (see figs. 9D and 9E).

5. Discussion

5.1 Mass transport-related liquefaction/fluidization: processes and products

Within the analyzed slide masses liquefaction/fluidization-related structures generally develop above a main, basal shear zone and, depending on the mechanical coupling between sliding mass and substrate, also into the underlying succession.

Evidence of liquefaction/fluidization processes is the sedimentary matrix represented by an unsorted, hyper-concentrated mixture of loose and poorly consolidated fine-grained sediments. This element is a fundamental component of a slide body along with other discrete parts that behave coherently (*e.g.* slide blocks, un-dissociated masses, *etc.*), usually marking the internal and basal shear zones as discontinuous or continuous, cm- to m-sized (and up to tens of m-sized) elongated lenses and bands, respectively.

Our data suggest that the basic deformation mechanism is the high-rated, generalized shearing of undrained (i.e. water saturated, low-permeability) sediments at low confining stress and fluid overpressure conditions. Besides the herein proposed process, instantaneous frictional heating is another possible mechanism able to cause increase pore pressure up to liquefaction (Goren and Aharonov, 2007).

As observed from both outcrop and geophysical data, most of the shearing achieved during the slide movement is likely accommodated within the basal interval, resulting in a sort of “overpressured carpet” that mechanically separates the slide mass from the substrate due to hampered hydraulic diffusivity. These overpressured basal interval are represented in a mass transport deposits by the lower matrix-dominated portions on outcrop and by the high-amplitude, inverse polarity reflectors on seismic profiles.

When the mechanical coupling becomes strong enough (*e.g.* during slide mass deceleration and freezing), the momentum can then be partly transferred downward, with the consequent involvement of the underlying sediments. This deformation is likely caused by dynamic/static overloading and rear push of the sliding mass. A similar geophysical evidence of this kind of mass transport-induced substrate deformation and incorporation (i.e. erosion in sedimentological meaning) is for instance shown by the high-resolution seismic profiles of small-scale lacustrine mass transport deposits provided by Schnellmann *et al.* (2005).

At the scale of the entire slide mass, compressional stress is mainly located at the front of the slide mass and then, transferred to the surrounding sediments. Folding and thrusting at various scales are the most common structural evidence of these processes in outcrops. The external arrangement of the final mass transport deposit is therefore characterized by low- to high-angle thrusts, isolated and/or rooted in the basal shear plane (*i.e.* blind thrusting), forming meso- to mega-scale folds which culminations may deform the upper surface forming elongated topographic highs (*e.g.* “pressure ridges”). At this scale, these shear zones seem to develop some kind of “backstepping” trend, following the upslope migration of the deformation kink-point due to the progressive stopping of slide mass front and margins.

During the emplacement, the extensional structures achieved during the failure and transport phases are thus likely overprinted and/or reworked in a generally compressive regime, as suggested by the predominance of compressional features recorded in the outcrop database.

5.2 Post-depositional processes and consequences

It is important to note that post-depositional processes seem to play a major role in the final anatomy of a slide body, as observed on ancient (Strachan, 2002, 2008) modern examples (Diviacco *et al.,* 2006; Moernaut *et al.*, 2009; Rebesco *et al.*, 2009;) and inferred from experimental and numerical modeling (Major and Iverson, 1999; Major, 2000). During the early post-depositional compaction, the internal fluid overpressure may be dissipated through developing of fluid-escape structures, sometimes reaching the slide surface as mud/sand volcanoes, or can be retained for a relatively long time interval, favoring slow differential movements of the entire mass. Such later movements develop as a generalized creeping of the upper surface of the slide deposit, with decreasing displacement towards its bottom, reworking and crosscutting earlier stage structures.

If the boundary conditions are favorable (*e.g.* slope steepness, weak layers in the substrate prone to liquefy, *etc.*) the frontal impact of a slide mass against seafloor highs or preceding landslide accumulations, and secondary movements of the deposit during the post-depositional stage may reactivate the material accumulated at the front of the body causing another secondary slide to start ("progressive landsliding"). This is well expressed in the frontal part of the Poverty mass transport complex, where the impact of secondary events has had a significant impact on the surface morphology and the internal structure of the landslide complex. Towards the upper portion of the slide, where extensional deformation may be expected repeated blocky failures impacting the upper slide debris have formed a zone dominated by large scale compressional deformation and thrust faulting. Towards the distal end of the landslide, where compression may be expected and particularly in frontally confined landslides, the landslide body shows widespread extension related to remobilization of the debris interpreted to occur in response to compressional impacts in the upper slide mass (fig. 10b). Further complicating this framework, smaller, secondary slide events, mainly in form of flows, may occur on the upper surface of slide masses, during the transport, accumulation and post-depositional stages.

5.3 Conceptual model of the internal mass transport deposit deformation

Combining the observations made on the two investigated mass transport deposits we tentatively propose a conceptual model of the deformation mechanisms acting within the slide mass, from up-slope to down-slope, on the basis of the amount of sedimentary matrix and its dominant position within the deposit. This model is represented in fig. 11.

In this framework the bulk of the deformation (both within the slide mass and in the underlying substrate) and the consequent *loci* of enhanced matrix production is supposed to be located where the slope gradient of the basal shear interval changes (e.g. flat-ramp transition, slope-basin transition, intra-basinal or intra-slope seafloor morphology).

It is important to point out that the described slide masses evolve within a morphologically confined setting. The resulting internal deformation and related structures are thus strongly influenced by the forced frontal and lateral compression/transpression with the intrabasinal highs, slide levees and the other preceding slide deposits. In a relatively unconfined depositional context, such as a foredeep basin plain, the frontal part of the slide mass could instead virtually spread out over long distances with the resulting development of mainly extensional/transtensional structures at the top of the slide masses (Lucente and Pini, 2003). Similar characteristics have been also observed in the morpho-bathymetric and seismic profiles of Eastern Mediterranean Slope, where frontally-confined and frontally-emergent mass transport complexes have been described (Frey-Martinez *et al.*, 2006).

Further work is planned to include in the model the lateral variations in the deformation style of the slide anatomy due to structural confinement.

6. Conclusions

Seismic reflection data reveal large-scale characteristics of emplacement processes in a complete mass transport complex, whereas outcrop analyses provide subtle details of controlling failure processes. The integration of the two different approaches is crucial for the correct understanding of the submarine landslide dynamics. Our key results are summarized as follows:

1) Liquefaction, fluidization and soft-sediment deformation are common processes in the internal structural evolution of submarine landslide bodies. The final product of such processes is an overpressured sedimentary matrix localized within discrete shear zones, which accommodate internal and basal friction forces, eventually enhancing slide mobility.

2) The main mechanisms invoked are a combination of (i) undrained shearing of water-saturated, poorly-consolidated sediments due to dragging forces acting along internal elements' boundaries (internal differential movements) and at the very base of the slide mass (down-slope movement), and (ii) dynamic loading and un-loading cycles due to the pulsating nature of the mass transport events.

3) At the scale of the entire deposit, such zones of concentrated fluid excess pore pressure can be visualized in seismic profiles, especially at the very base of the unit where horizons of trapped high fluid pressure may induce high amplitude reflectivity and even negative polarity. Such reflectors can be observed also within the slide mass, and depending on their lateral continuity, may indicate the amalgamation surface/interval between two subsequent bodies, therefore representing a powerful tool to distinguish single depositional units (mass transport deposits) from composite, multiple accumulation complexes (mass transport complexes).

4) The whole slide mass can be longitudinally subdivided into different zones characterized by different stress regime and consequent deformation mechanisms, as evidenced by the different relative amount of sedimentary matrix.

The systematic integration of available geophysical data with detailed outcrop studies represents the most reliable method for the study of submarine landslides. This synergic approach permits observations covering all the scales (from the microscopic to the regional scale) and allows overcoming the intrinsic resolution limits of the single methods. Accordingly, the hypotheses coming from the modern marine geology surveys can be tested and calibrated directly on selected analogues on the field, and *vice versa*, especially in terms of genetic and evolutionary processes and slide dynamics, which in turn represent the key factors that control forecasting and mitigation of submarine landslide-related geohazards.

Acknowledgments

We would like to thank Hans-Juergen Gawlick, Dusan Plasienka and an anonymous reviewer for having deeply improved the quality of the manuscript with their constructive comments and suggestions. Joshu Mountjoy supported by NIWA under Coasts and Oceans Research Programme 1 (2013/14 SCI).

References

Alsop, G.I., Holdsworth, R.E. 2004. The geometry and topology of natural sheath folds: a new tool for structural analysis - Journal of Structural Geology, v. 26, 1561–1589.

Barker, D.H.N., Sutherland, R., Henrys, S., Bannister, S., 2009. Geometry of the Hikurangi subduction thrust and upper plate, North Island, New Zealand. Geochem. Geophys. Geosyst., 10.

Barnes, P.M., Lamarche, G., Bialas, J., Henrys, S., Pecher, I.A., Netzeband, G.L., Greinert, J., Mountjoy, J.J., Pedley, K., Crutchley, G., 2010. Tectonic and Geological Framework for Gas hydrates and Cold Seeps on the Hikurangi Subduction Margin, New Zealand. Marine Geology 272(1-4), 26-48.

Bradley, D., Hanson, L., 1998. Paleoslope Analysis of Slump Folds in the Devonian Flysch of Maine. Journal of Geology 106, 305–318.

Bull, S., Cartwright, J., 2010. Small-Scale Insights into Seismic-Scale Slumps: A Comparison of Slump Features from the Waitemata Basin, New Zealand, and the Møre Basin, Off-Shore Norway. In D.C. Mosher *et al.* (Eds.), Submarine Mass Movements and Their Consequences, 257 Advances in Natural and Technological Hazards Research 28, 257-266.

Bull, S., Cartwright, J., Huuse, M., 2009. A review of kinematic indicators from mass-transport complexes using 3D seismic data. Marine and Petroleum Geology 26/7, 1132-1151.

Callot, P., Odonne, F., Sempere, T., 2008a. Liquification and soft-sediment deformation in a limestone megabreccia: The Ayabacas giant collapse, Cretaceous, southern Peru. Sedimentary Geology 212, 49–69.

Callot, P., Sempere, T., Odonne, F., Robert, E., 2008b. Giant submarine collapse of a carbonate platform at the Turonian-Coniacian transition: The Ayabacas Formation, southern Peru. Basin Research 20, 333–357. doi: 10.1111/j.1365-2117.2008.00358.x.

Canals, M., Lastras, G., Urgeles, R., Casamor, J.L., Mienert, J., Cattaneo, A., De Batist, M., Haflidason, H., Imbo, Y., Laberg, J.S., Locat, J., Long, D., Longva, O., Masson, D.G., Sultan, N., Trincardi, F., Bryn, P., 2004. Slope failure dynamics and impacts from seafloor and shallow sub-seafloor geophysical data: case studies from the COSTA project. Marine Geology 213, 9-72.

Castellarin, A., 1994. Strutturazione eo-mesoalpina dell'Appennino Settentrionale attorno al "nodo ligure. In: Capozzi, R., Castellarin, A. (Eds.), Studi preliminari all'acquisizione dati del profilo CROP 1–1A La Spezia–Alpi orientali. Studi Geologici Camerti, Volume Speciale 1992/2: Camerino, Università degli Studi di camerino, 99-108.

Cavazza, W., Roure, F., Ziegler, P.A., 2004. The Mediterranean area and the surrounding regions: active processes, remnants of former Tethyan oceans and related thrust belts. In: Cavazza, W., Roure, F., Spakman, W., Stampfli, G.M., Ziegler, P.A. (Eds.), The TRANSMED Atlas: The Mediterranean Region from crust to mantle. Springer, 1–29.

Di Giulio, A., Mancin, N., Martelli, L., 2002. Geohistory of the Ligurian orogenic wedge: first inferences from Epiligurian sediments. Boll. Soc. Geol. It., Spec. vol. 1, 375-384.

Diviacco, P., Rebesco, M., Camerlenghi, A., 2006. Late Pliocene mega debris flow deposit and related fluid escapes identified on the Antarctic Peninsula continental margin by seismic reflection data analysis. Marine Geophysical Research 27, 109–128.

Festa, A., Dilek, Y., Pini, G.A., Codegone, G., Ogata, K., 2012. Mechanisms and processes of stratal disruption and mixing in the development of mélanges and broken formations: Redefining and classifying mélanges. Tectonophysics 568-569, 7-24, doi: 10.1016/j.tecto.2012.05.021.

Festa, A., Pini, G.A., Dilek, Y., Codegone, G., 2010a. Mélanges and mélange-forming processes: a historical overview and new concepts, in: Dilek, Y. (Ed.), Alpine Concept in Geology. Int. Geol. Rev. 52 (10-12), 1040-1105, doi: 10.1080/00206810903557704.

Festa, A., Pini, G.A., Dilek, Y., Codegone, G., Vezzani, L., Ghisetti, F., Lucente, C.C., Ogata, K., 2010b. Peri-Adriatic mélanges and their evolution in the Tethyan realm, in: Dilek, Y. (Ed.), Eastern Mediterranean geodynamics (Part II). Int. Geol. Rev. 52 (4-6), 369-406, doi: 10.1080/00206810902949886.

Frey-Martinez, J., Cartwright, J., James, D., 2006. Frontally confined versus frontally emergent submarine landslides: a 3D seismic characterization. Marine and Petroleum Geology 23, 585-604.

Gee, M.J.R., Uy, H.S., Warren, J., Morley, C.K., Lambiase, J.J., 2007. The Brunei slide: A giant submarine landslide on the North West Borneo Margin revealed by 3D seismic data. Marine Geology 246/1, 9-23.

Goren, L., Aharonov, E. 2007. Long run-out landslides: the role of frictional heating and hydraulic diffusivity. Geophysical Research Letters 34, 1-7.

Goren, L., Aharonov, E., Sparks, D., Toussaint, R. 2010. Pore pressure evolution in deforming granular material: A general formulation and the infinitely stiff approximation, J. Geophys. Res. 115, B09216.

Goren, L., Aharonov, E., Sparks, D., Toussaint, R. 2011. The Mechanical Coupling of Fluid-Filled Granular Material Under Shear. Pure and Applied Geophysics 168, 10.1007/s00024-011-0320-4.

Hampton, M.A., Lee, H.J., Locat, J., 1996. Submarine Landslides. Rev Geophys 34, 33-59.

Kawamura, K., Sasaki, T., Kanamatsu, Y., Arito, S., Ogawa, Y., 2012. Large submarine landslides in the Japan Trench: A new scenario for additional tsunami generation. Geophys Res Lett 39, L05308

Knipe, R.J., 1986. Deformation mechanism path diagrams for sedi- ments undergoing lithification. In: Moore, J. C. (Ed.), Structural Fabrics in D. S. D. P. Cores from Forearcs. Mem. geol. Soc. Am. 166, 151-160.

Lamarche, G., Joanne, C., Collot, J.-Y., 2008. Repetitive Large Submarine Mass Transport Complexes in the South-Kermadec Forearc Basin: The Matakaoa

Submarine Instability System. Geochemistry Geophysics Geosystems 9(4), Q04001.

Lewis, K.B., Pettinga, J.R., 1993. The emerging, imbricate frontal wedge of the Hikurangi margin. In: Ballance P.F. (Ed.), South Pacific sedimentary basin. Sedimentary Basins of the World 2. Elsevier Sciences publishers, Amsterdam, pp. 225-250.

Lucente, C.C., Pini, G.A. 2003. Anatomy and emplacement mechanism of a large submarine slide within a Miocene foredeep in the Northern Appennines, Italy: a field perspective. American Journal of Science 303, 565-602.

Macdonald, D.I.M, Moncrieff, A.C.M., Butterworth, P.J., 1993. Giant slide deposits from a Mesozoic fore-arc basin, Alexander Island, Antarctica. Geology 21/11, 1047-1050.

Major, J.J., 2000. Gravity-driven consolidation of granular slurries: implications for debris-flow deposition and deposit characteristics. Journal of Sedimentary Research 70/1, 64-83.

Major, J.J., Iverson, R.M., 1999. Debris-flow deposition: effects of pore-fluid pressure and friction concentrated at flow margins. GSA Bulletin 111, 1424–1434.

Marroni, M., Meneghini, F., Pandolfi, L., 2010. Anatomy of the Ligure-Piemontese subduction system: evidence from Late Cretaceous–middle Eocene convergent margin deposits in the Northern Apennines, Italy. Int. Geol. Rev. 52, 1160-1192.

Martelli, L., Cibin, U., Di Giulio, A., Catanzariti, R., 1998. Litostratigrafia della Formazione di Ranzano (Priaboniano sup.-Rupeliano, Appennino Settentrionale e Bacino Terziario Ligure Piemontese). Boll. Soc. Geol. It., vol. 117, 151-185.

Middleton, G.V., Hampton, M.A., 1973. Sediment gravity flows: mechanics of flow and deposition. - In. Middleton G.V., Bouma, A.H. (Eds.), Turbidites and Deep-water Sedimentation. SEPM Pacific Section, Short Course Notes, 1-38.

Moernaut, J., De Batist, M., Heirman, K., Van Daele, M., Pino, M., Brümmer, R., Urrutia, R., 2009. Fluidization of buried mass-wasting deposits in lake sediments and its relevance for paleoseismology: results from a reflection seismic study of lakes Villarrica and Calafquén (South-Central Chile). Sedimentary Geology 213, 121–135.

Mosher, D.C., Austin, J.A. Jr., Fisher, D., Gulick, S.P.S., 2009. Deformation of the northern Sumatra accretionary prism from high-resolution seismic reflection profiles and ROV observations. Marine Geology 252, 89–99.

Mountjoy, J., Barnes, P., Pettinga, J., 2009. Morphostructure of submarine canyons on an active margin: Cook Strait Canyon system, New Zealand. Marine Geology 260, 45–68. doi:10.1016/j.margeo.2009.01.006.

Mountjoy, J.J., Barnes, P.M., 2011. Active upper-plate thrust faulting in regions of low plate-interface coupling, repeated slow slip events, and coastal uplift: Example from the Hikurangi Margin, New Zealand. Geochem. Geophys. Geosyst., 12, Q01005. doi:10.1029/2010GC003326.

Mountjoy, J.J., Micallef, A., 2012. Polyphase Emplacement of a 30 km3 Blocky Debris Avalanche and Its Role in Slope-Gully Development. In: Y. Yamada, K. Kawamura, K. Ikehara, Y. Ogawa, R. Urgeles, D. Mosher, J. Chaytor, M. Strasser (Eds.), Submarine Mass Movements and Their Consequences. Advances in Natural and Technological Hazards Research. Springer, Netherlands, pp. 213-222.

Mulder, T., Alexander, J., 2001. The physical character of subaqueous sedimentary density flows and their deposits. Sedimentology 48, 269-299.

Mutti, E., Carminatti, M., Moreira, J.L.P., Grassi, A.A., 2006. Chaotic Deposits: examples from the Brazilian offshore and from outcrop studies in the Spanish Pyrenees and Northern Apennines, Italy. A.A.P.G. Annual Meeting, April 9-12, Houston, Texas.

Mutti, E., Papani, L., Di Biase, D., Davoli, G., Mora, S., Segadelli, S., Tinterri, R., 1995. Il Bacino Terziario Epimesoalpino e le sue implicazioni sui rapporti tra Alpi ed Appennino. Memorie di Scienze Geologiche di Padova 47, 217 – 244.

Mutti, E.,1992. Turbidite Sandstones. San Donato Milanese, Agip-Istituto di Geologia, Università di Parma, 275 pp.

Ogata, K., Mutti, E., Pini G.A., Tinterri, R., 2012a. Mass transport-related stratal disruption within sedimentary mélanges. Tectonophysics 568-569, 185-199.

Ogata, K., Tinterri, R., Pini, G.A., Mutti, E., 2012b. The Specchio Unit (Northern Apennines, Italy): an ancient mass transport complex originated from near-coastal areas in an intra-slope setting. In: Yamada, Y., Kawamura, K., Ikehara, K., Ogawa, Y., Urgeles, R., Mosher, D., Chaytor, J., Strasser, M. (Eds.), Submarine Mass Movements and Their Consequences. Advances in Natural and Technological Hazards Research. Springer Netherlands, 595-605.

Orpin, A.R., 2004. Holocene sediment deposition on the Poverty-slope margin by the muddy Waipaoa River, East Coast New Zealand. Marine Geology 209, 69-90.

Passchier, C.W., Trouw, R.A., 2005. Microtectonics. Springer Berlin Heidelberg New York, 365 pp.

Pedley, K.L., Barnes, P.M., Pettinga, J.R., Lewis, K.B., 2010. Seafloor structural geomorphic evolution of the accretionary frontal wedge in response to seamount subduction, Poverty Indentation, New Zealand. Marine Geology 270(1-4), 119-138.

Pini, G.A., Ogata, K., Camerlenghi, A., Festa, A., Lucente, C.C., Codegone, G., 2012. Sedimentary mélanges and fossil mass-transport complexes: a key for better under- standing submarine mass movements? In: Yamada, Y., Kawamura, K., Ikehara, K., Ogawa, Y., Urgeles, R., Mosher, D., Chaytor, J., Strasser, M. (Eds.), Submarine Mass Movements and Their Consequences. Advances in Natural and Technological Hazards Research. Springer Netherlands, 585-594.

Pini, G.A.,1999. Tectonosomes and olistostromes in the Argille Scagliose of the Northern Apennines, Italy. Geol. Soc. of America Special 335, 73 pp..

Pouderoux, H., Lamarche, G., Proust, J.N., 2012. Building an 18 000-year-long paleo-earthquake record from detailed deep-sea turbidite characterisation in Poverty Bay, New Zealand. Nat Hazard Earth Sys, 12(6), 2077-2101.

Rebesco, M., Neagu, R.C., Cuppari, A., Muto, F., Accettella, D., Dominici, R., Cova, A., Romano, C., Caburlotto, A., 2009. Morphobathymetric analysis and evidence of submarine mass movements in the western Gulf of Taranto (Calabria margin, Ionian Sea). Int. J. Earth Sci. (Geol. Rundsch.) 98, 791–805. DOI 10.1007/s00531-009-0429-1

Schnellmann, M., Anselmetti, F. Giardini, D., McKenzie, J. 2005. Mass movement-induced fold-and-thrust belt structures in unconsolidated sediments in Lake Lucerne (Switzerland). Sedimentology 52, 271–289. doi: 10.1111/j.1365-3091.2004.00694.x

Strachan, L.J., 2002. Slump-initiated and controlled syndepositional sandstone remobilization: an example from the Namurian of County Clare, Ireland. Sedimentology 49, 25-41.

Strachan, L.J., 2008. Flow transformations in slumps: a case study from the Waitemata Basin, New Zealand. Sedimentology 55, 1311–1332.

Strachan, L.J., Alsop, G.I., 2006. Slump folds as estimators of palaeoslope: a case study from the Fisherstreet Slump of County Clare, Ireland. Basin Research 18, 451-470.

Vardy, M.E., L'Heureux, J.-S., Vanneste, M., Longva, O., Steiner, A., Forsberg, C.F., Haflidason, H., Brendryen, J. 2012. Multidisciplinary investigation of a shallow near–shore landslide, Finneidfjord, Norway. Near Surface Geophysics 10(4), 267-277. (doi:10.3997/1873-2012022).

Walsh, J.P., Alexander, C.R., Gerber, T., Orpin, A.R., Sumners, B.W., 2007. Demise of a submarine canyon? Evidence for highstand infilling on the Waipaoa River continental margin, New Zealand. Geophysical Research Letters 34, L20606.

Woodcock, N.H., 1979. The use of slump structures as palaeoslope orientation estimators. Sedimentology 26/1, 83 – 99.

Yamada, Y., Kawamura, K., Ikehara, K., Ogawa, Y., Urgeles, R., Mosher, D., Chaytor, J., Strasser, M. (Eds.), 2012. Submarine Mass Movements and Their Consequences. Advances in Natural and Technological Hazards Research, Springer Netherlands.

Figure caption

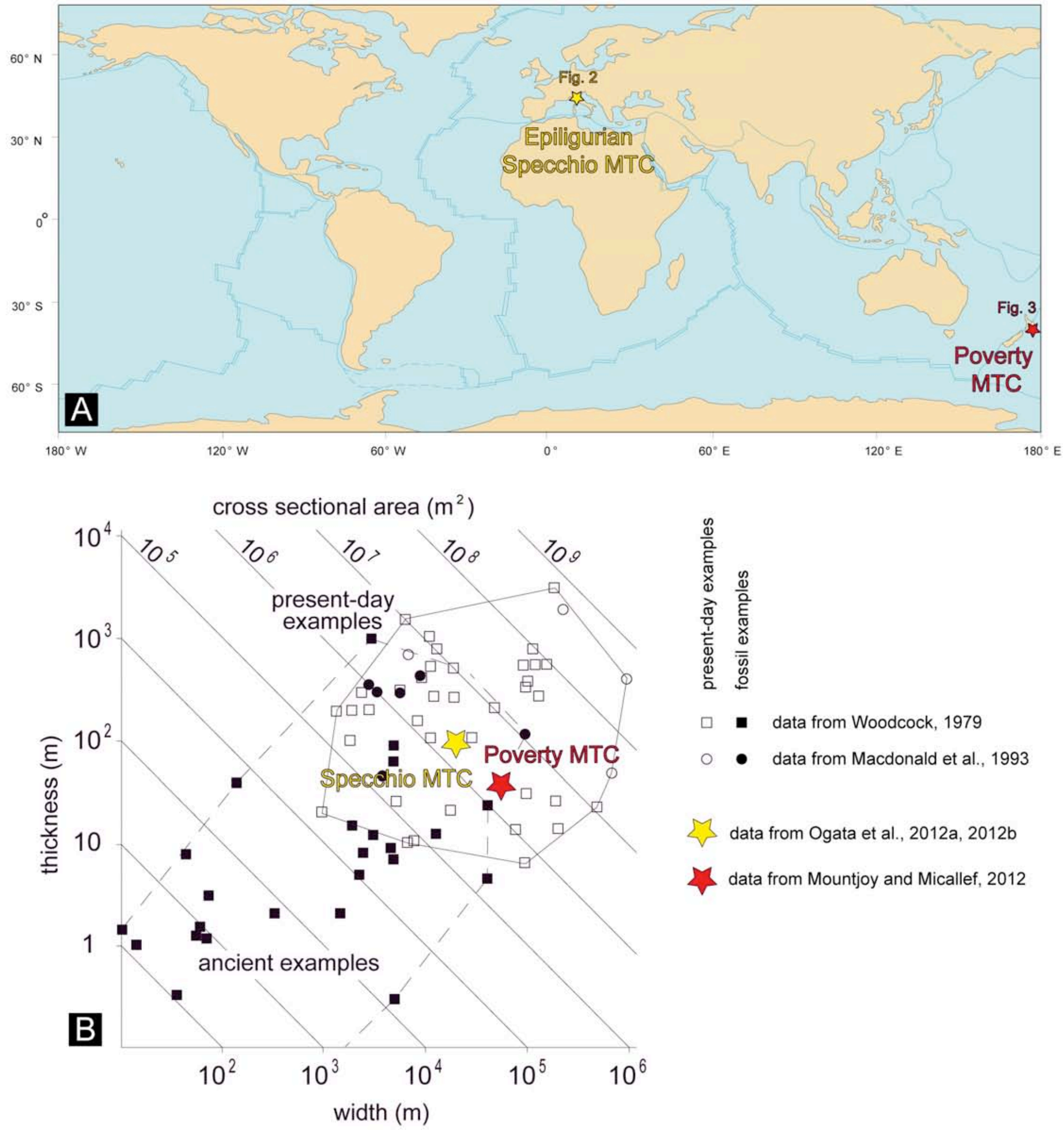

Average component MTDs	Length (km)	Width (km)	Area (km2)	Volume (km3)	Depth range (m)	Max. thickness (m)	Component MTDs (Nr.)	Slide element max. cross-sectional length (m)	Internal characteristics	External morphology	Depositional Setting	Source area	Reference
Specchio MTC	45*	20*	380*	75*	500-2000*	300	≥ 3	up to 200	Bipartite deposit with a slump-like, block-dominated upper part and a debris flow-like, matrix-dominated lower part	Uneven upper surface draped by turbidite-type deposits and strongly erosive basal surface. High lateral thickness variability and amalgamations.	Intra-slope, wedge top, confined basin system	shelf-shelf edge-upper slope	Ogata, 2010
Poverty MTC	35	15	250	33.5	1100-1500	250	≥ 2	up to 500-1000	Weak, semi continuous coherent reflectors separated by transparent to faintly reflective zones	Irregular blocky upper surface roughness with longitudinal variations, with larger blocks in the upslope part and smaller blocks in the downslope part. Strongly erosive basal surface. High lateral thickness variations.	Intra-slope, wedge-top, confined fore-arc basin	upper slope	Mountjoy and Micallef, 2012

C

*based on extrapolation of field observations

Figure 1: A) Geographic location of the two case studies. B) Thickness vs. width diagram showing relative sizes of ancient (dashed line envelope) and present-day (solid line envelope) mass transport deposits (MTDs) and mass transport complexes (MTCs). The relative dimensions o the two studied examples are

plotted. Modified from Lucente and Pini (2003) after Woodcock (1979) and Macdonald et al. (1993). C) Table listing the parameters of comparison between the two analyzed examples: the Specchio MTC (Italy) and the Poverty MTC (New Zealand).

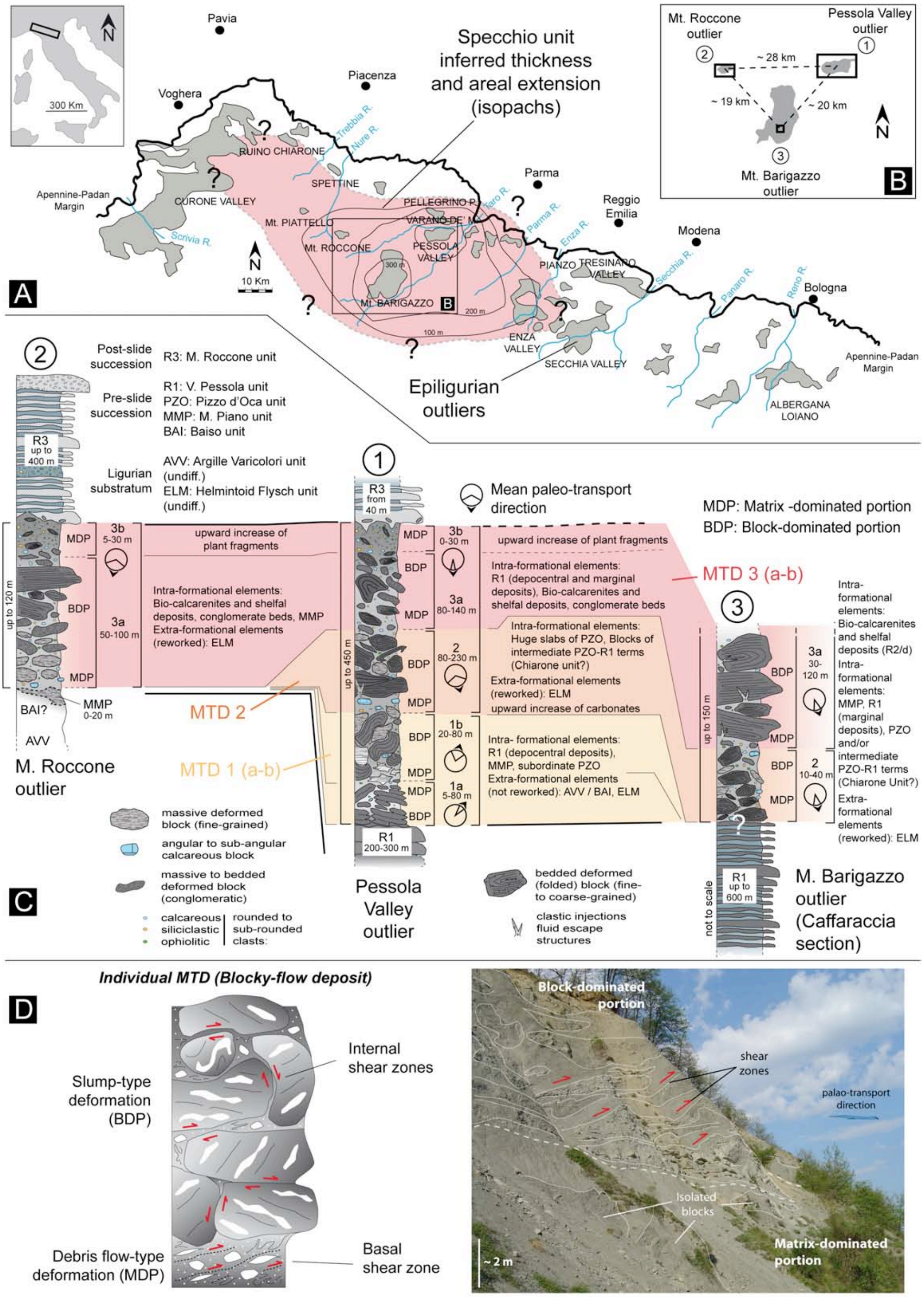

Figure 2: A) Schematic representation of the sedimentary remnants (i.e. outliers) of the Epiligurian succession scattered across the eastern side of the Northern Apennines (location in the left inset). Redrawn and modified from Martelli et

al. (1998). B) Close up of A showing the reciprocal distances and location of the three Epiligurian outliers (i.e. Pessola Valley, Mt. Roccone and Mt. Barigazzo sections) where the Specchio MTC has been investigated. C) Simplified stratigraphic logs and correlation of the Specchio MTC across the three investigated Epiligurian outliers (location in B). The internal subdivisions, lithologies, main component and mean paleo-transport directions are labeled (modified after Ogata et al., 2012a, 2012b). D) Schematic log of a blocky flow deposits, showing the basic component MTD of the Specchio unit. In the photograph a line drawing of the MTD 2 (see C) labeling the main structural elements is depicted.

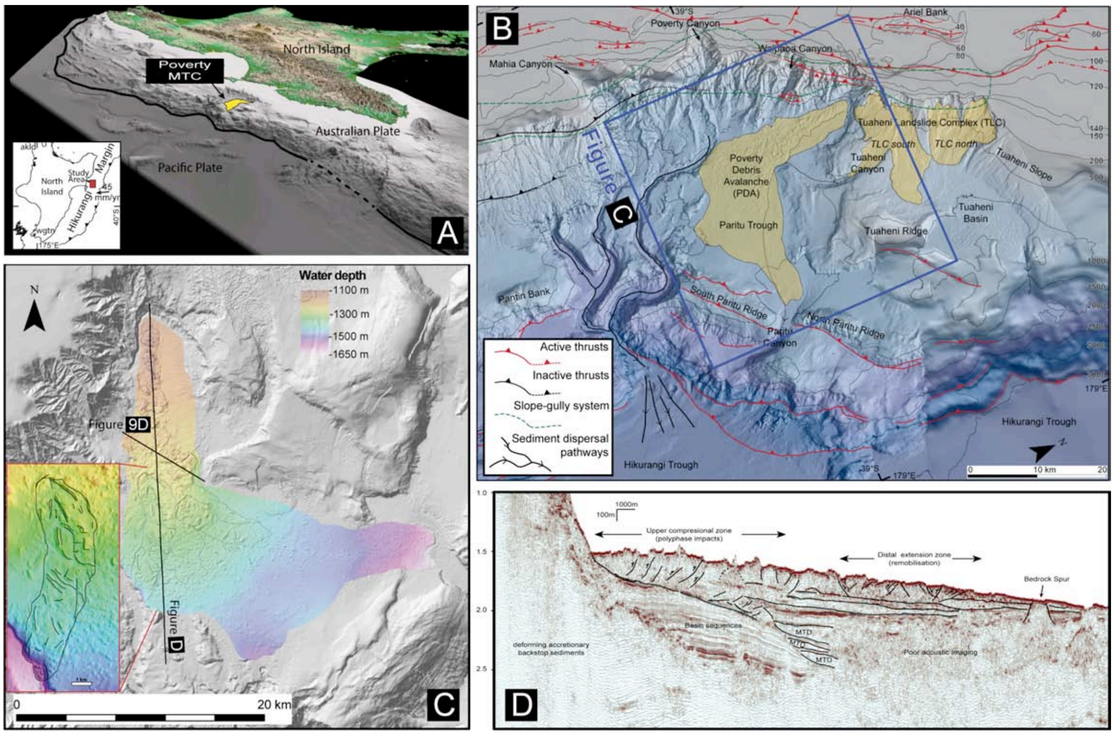

Figure 3: A) Bird's eye view of the northeastern continental margin of New Zealand (looking toward the SW; location of the area in the inset). Plate boundaries and position of the investigated Poverty MTC are labeled. B) Interpreted geomorphic map of the upper Poverty Re-entrant showing the main MTDs (labeled in yellow) and the major characterizing structures (see explanation

inset). C) Morphologic map of the Poverty MTC with water-depth ranges indicated. The inset shows a secondary superficial failure (i.e. subordinate MTD) affecting the frontal part of the main MTD. MCS profiles' paths shown in D and Fig. 9D are labeled. D) Internal stratigraphy of the Poverty MTC and host sedimentary succession as resolvable in MCS data. The entire length of the Poverty MTC is covered, showing in particular 1) an upslope compressional part and a downslope extensional part (labeled) due to base-of-slope accumulation, 2) a complex basal flat-ramp erosional surface (basal solid line) and 3) weak, discontinuous internal reflectors suggesting the amalgamation of at least 2 main depositional events (internal solid lines). In addiction, the underlying sedimentary succession is characterized by the occurrence of at least 3 other MTDs testifying that submarine landsliding is a recurrent process in this setting.

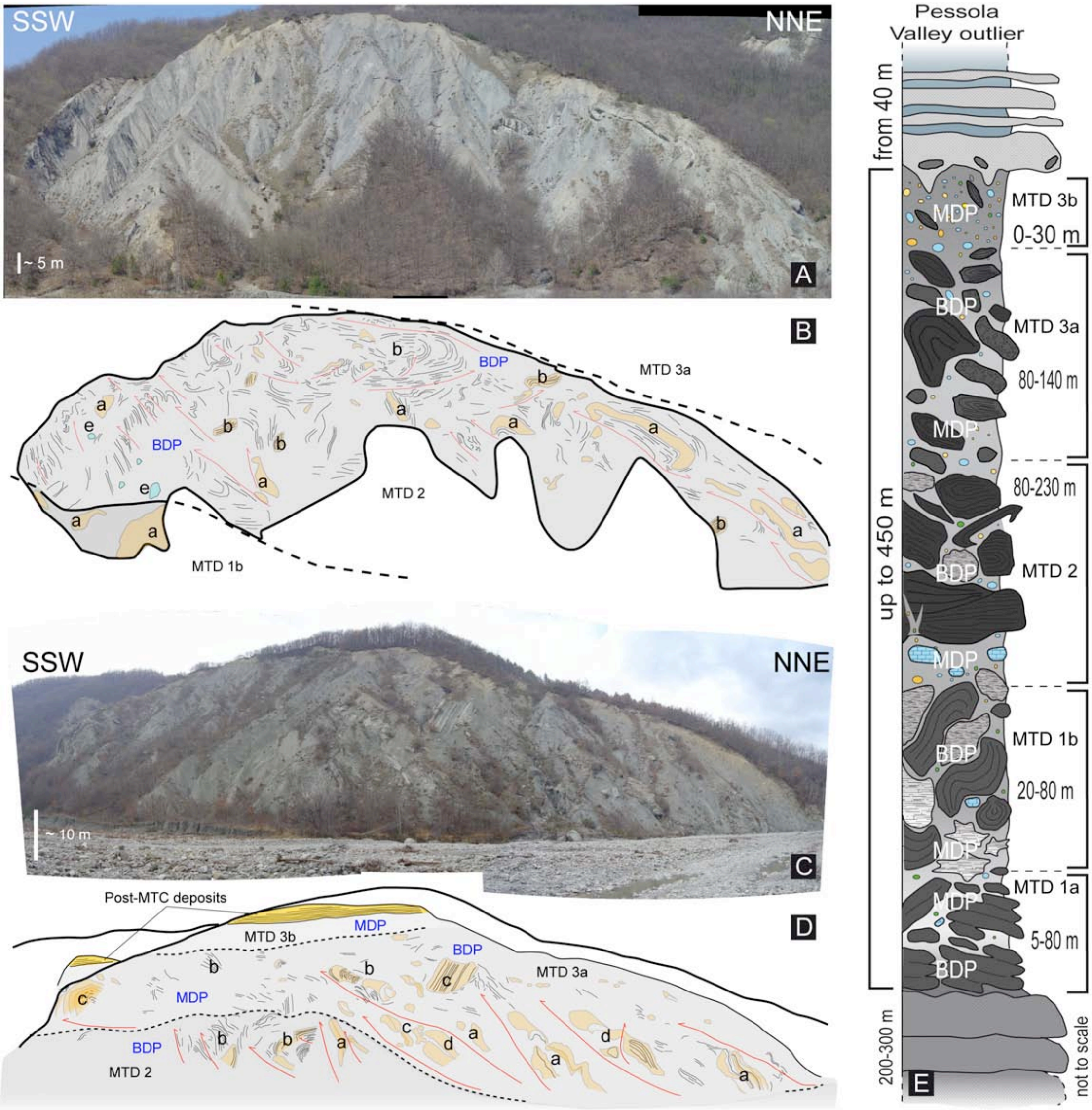

Figure 4: Early Rupelian Specchio MTC (Pessola Valley section). A) Photomosaic of the middle component (MTD 2) of the Specchio unit. B) Interpretation and line drawing of the recognizable internal bedding (black lines). C) Photomosaic of the upper component (MTD 3) of the Specchio unit. D) Interpretation and line drawing of the main structures. E) Simplified stratigraphic column of the Specchio MTC in the type locality in the Pessola Valley outlier. The component MTDs and the relative thickness ranges are indicated. Explanation of labels in B and D: a - thick-bedded, coarse-grained sandstone elements; b - thin-bedded, fine-grained sandstone-mudstone

elements; c - medium-bedded, fine- to medium-grained sandstone-siltstone elements; d - pebbly to cobbly conglomerate elements; e - carbonate elements; MDP - matrix-dominated portion; BDP - block-dominated portion.

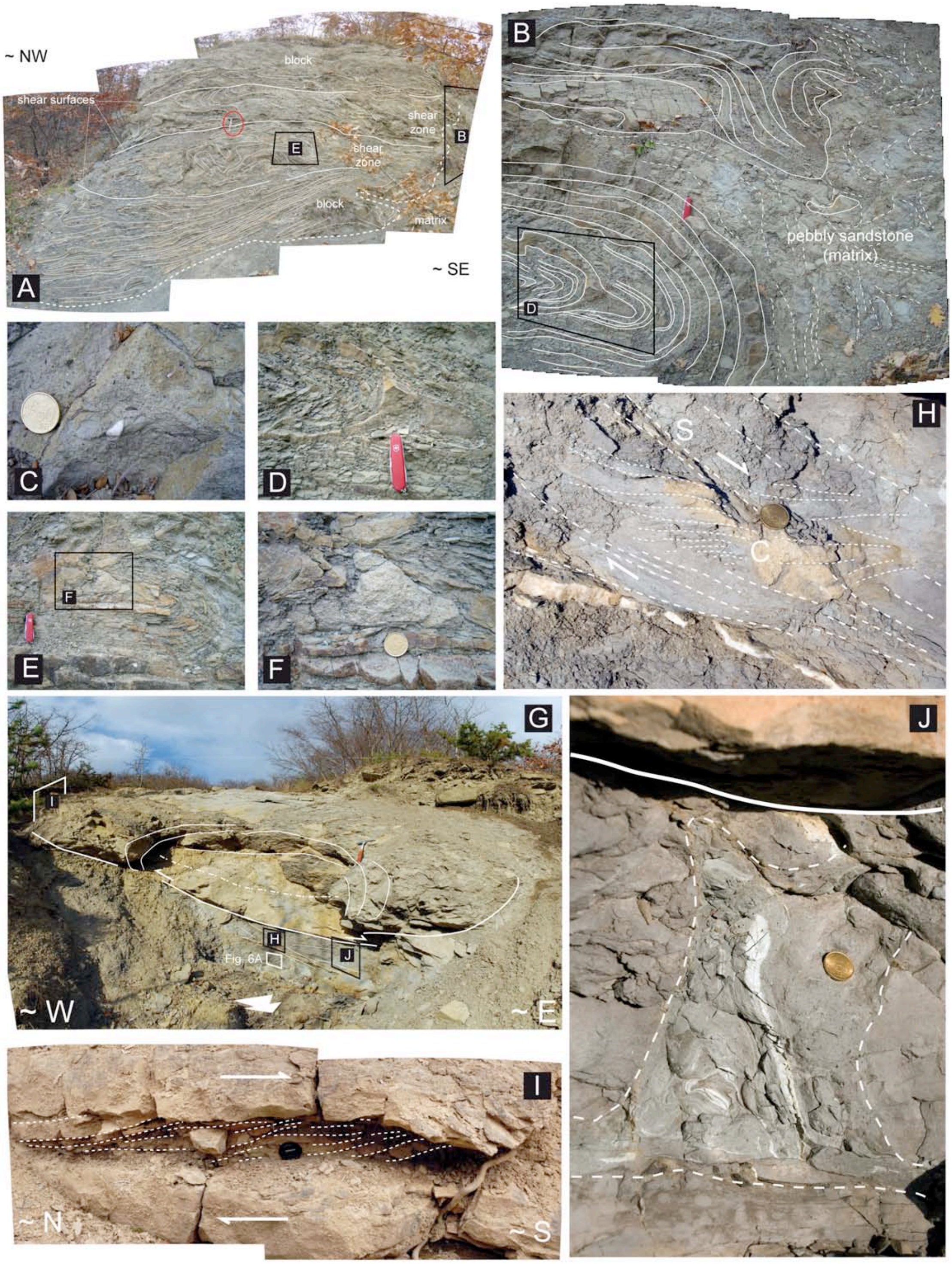

Figure 5: Early Rupelian Specchio MTC (Mt. Roccone section), MTD 2. A) Photomosaic and line drawing of ductile-like shear zones affecting a slide

block made up of thin-bedded sandstone-mudstone interlayers. Circled hammer for scale. B) Close-up of A showing the soft sediment folds (solid lines) and the fluidal structures within the host sedimentary matrix (dashed lines) at the slide block lateral boundary (location in A). This matrix forms sub-horizontal injection into the slide block roughly along the termination of the shear planes labeled in A. C) Detail of the sedimentary matrix showing well-rounded pebbles and granules dispersed within a fine-grained unsorted sedimentary matrix containing well-rounded pebbles and granules dispersed within a clayey-marly lithology. D) Close-up of the isoclinal fold represented in B, showing the extreme, localized thickening of a cm-thick sandstone bed in the hinge zone, testifying liquefaction of the sandy material. E) Close-up of A showing an isoclinal synform fold with the upper limb truncated and matrix injection along the axial plane. F) Detail of E showing the injected matrix into the fold's hinge zone. G) A cm-thick shear zone (thick solid line and white arrows indicating the shear sense) overlain by a slide block made of thin-bedded, fine-gained sandstone layers (thin solid lines) plastically deformed into a meso-scale sheath fold (axis trend marked by dashed line). The white arrow indicates the mean paleo-transport direction inferred. H) Close-up of the shear zone in G showing the ductile-like, pseudo-SC shear structures (dotted lines). White arrows indicate the inferred shear sense. I) Detail of the shear zone in G showing sigmoidal-type structures and small-scale duplexes (dotted lines). The inferred shear sense is labeled (white arrows). J) Close up of the base of the slide block in G showing upward matrix injections (e.g. fluid escape) rooted in the shear zone. Note the fluidal structures defined by extremely plastically deformed marly intraclasts within the pebbly mudstone.

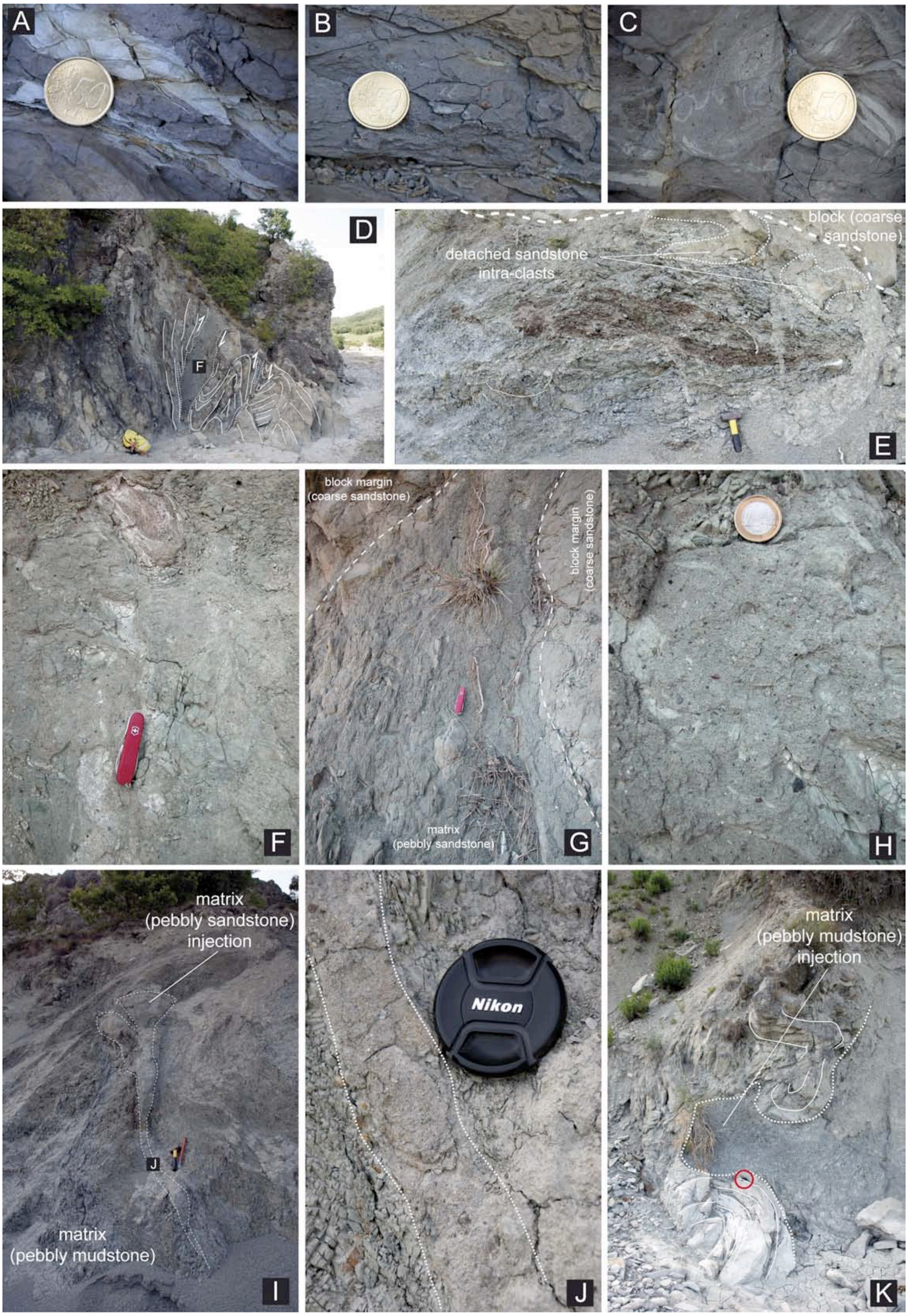
A
B
C
D
F
block (coarse sandstone)
detached sandstone intra-clasts
E
block margin (coarse sandstone)
block margin (coarse sandstone)
matrix (pebbly sandstone)
F
G
H
matrix (pebbly sandstone) injection
J
matrix (pebbly mudstone)
I
Nikon
J
matrix (pebbly mudstone) injection
K

Figure 6: Early Rupelian Specchio MTC (Pessola Valley and Mt. Roccone sections); lower-middle MTDs 2 and 3. A) Example of sedimentary matrix coming from a cm-thick shear zone (location in fig. 5G). Note the shearing-related, asymmetric boudinage of the marly intraclasts. B) Example of the unsorted, pebbly mudstone sedimentary matrix. Some elements, especially the elongated intraclasts, show a rough iso-orientation of the long axes. C) Example of the fluidal structures (e.g. hydroplastic folds) found within the sedimentary matrix shown in B. D) Thick (ca. 60 cm) shear zone marked by a discontinuous band of unsorted, mixed and generally massive pebbly sandstone in a sandy block-dominated portion. E) A detached isoclinal fold developed in an exotic (Cretaceous Ligurian AVV unit, see text) shaly slide block at the boundary between the matrix- and block-dominated portions. F) Detail of the shear zone in D showing the appearance of the pebbly sandstone matrix. Note the hydroplastically folded, fine sandstone and mudstone intraclasts. G) Matrix-rich shear zone developed at the lateral contact between two slide blocks within the block-dominated portion shown in D. The pebbly sandstone matrix displays pseudo-SC shears and rotated/deformed clasts characterized by pseudo-sigma shapes. H) Detail of the host pebbly sandstone/mudstone matrix characterizing the matrix-dominated portion. Note the overall alignment and the iso-orientation of the mudstone intraclasts. I) Dome-topped pebbly sandstone dyke injecting into the host pebbly mudstone matrix of the matrix-dominated portion in E. This structure suggests later (i.e. post-depositional) liquefaction of pressurized discrete sandy elements (i.e. slide blocks) with consequent intrusion into the more impermeable, compacting host pebbly mudstone matrix. J) Close up of I showing in detail the pebbly-sandy material

comprising the matrix injection. K) Dome-shaped lateral injection of host pebbly mudstone matrix into a sandstone block with associated plastic folding of the sandstone beds. Circled lens cap for scale.

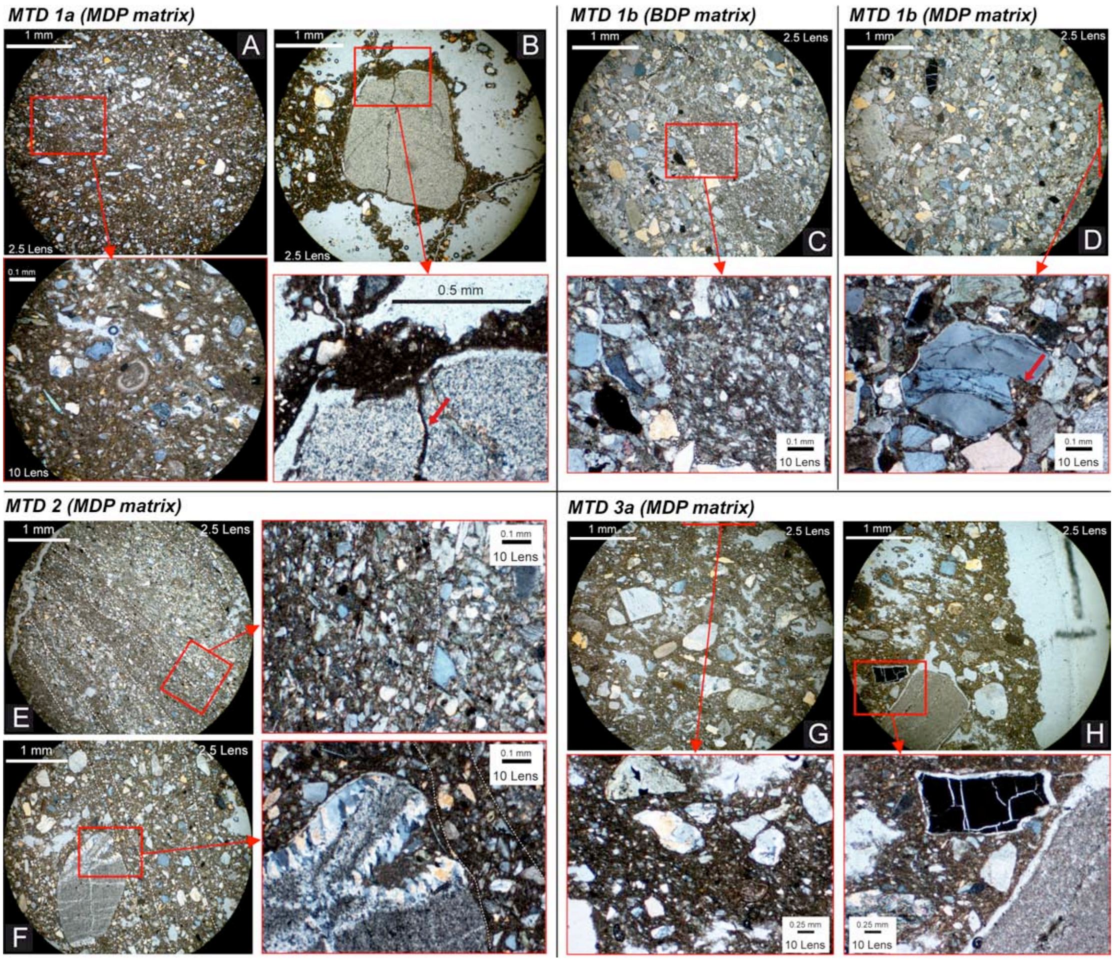

Figure 7: Early Rupelian Specchio MTC, optical microscope observations of the matrix for each component MTD. A) Fine-grained portions of the matrix showing the “brecciated” texture and the occurrence of both rounded and angular grains. Close-up: detail of the finer granulometric population of the matrix. Note the occurrence of well-preserved microfossils (radiolarians?) and the “fluidal” appearance of the finer matrix, enveloping grains and filling voids between elements. B) Sub-rounded lithic grain showing a fracture filled with finer material of the host matrix. Close-up: detail the injection of fine-grained matrix within the fracture (red arrow). This evidence indicates fluid

overpressure conditions of the matrix, possibly up to hydro-fracturing. C) Medium- to coarse-grained sand particles with mud infillings within inter-granular spaces. Elongated patches of fine-grained material, sharing the same characteristics of the muddy component are aligned to the overall oblique banding (from the upper-left to the lower-right), expressed by iso-orientation of grains' long axes and by elongated clustering of particles sharing similar dimensions. Close-up: detail of the transitional border of the fine-grained elongated patches with the surrounding matrix material. The fine-grained lithology is the same of that filling inter-granular spaces and sustaining sandy particles. Note the "fluidal" appearance of the fine-grained material and the development of faint planar discontinuity (e.g. psudo-foliation) marked by the preferential alignment of elongated/platy grains. D) Matrix with fine-grained material more diffused and diluted within the sandy grains, and lineations and banding less evident. The overall appearance is more "matrix-sustained" than that observed in C. Partial close up: detail of a fractured sub-angular quartz grain, characterized by a thin calcite halo, and surrounded by fine-grained material. The latter seems to inject into internal voids of the grain (red arrow); other minor injections along fractures are present. Along with this, the fine-grained material envelops particles (even where grains are almost in contact) testifying its plastic/fluidal nature. E) Matrix showing a thinly banded appearance. Note the fine-grained material arranged in "ribbon"-like patches. Lineations are also highlighted by the preferential alignment of particles, along their long axis. Close-up: boundary between two relatively fine- and coarse-grained elongated clusters. These structures suggest overall simple shear conditions achieved through an independent particulate flow without cataclasis (i.e. grain breakage) and, are here defined as pseudo-deformation/disaggreagation bands. F) Homogeneous unsorted matrix. The well-rounded, mm-sized, lithic pebble (metamorphic?) observable in the lower-left side of the photo is internally characterized by the intrusion of the finer material into the voids left by leached out, previously mineralized vein. Note also the faintly recognizable shear-like band passing tangentially to the upper-right margin of largest pebble, and trending obliquely the photo, from the upper-left side to the lower-right side (boundaries labeled with white dashed lines). Close-up: detail of the primary mineralized vein and the injected fine-grained material. This evidence supports the fluid-like state of the matrix. Note the fluidal-like appearance of the surrounding matrix, simulating pebble boundaries. G) Rigid particles dispersed and sustained within a fine-grained, unconsolidated lithology. Partial close-up: relationships between particles and the finer material, which envelopes grains and seems to be structurally arranged in a crude oblique lineation (deformation bands-like structures), as underlined by particles alignment. H) Overview of the matrix close to a major, mm-sized, well-rounded pebble of sedimentary origin. Close-up: detail the finer matrix surrounding the pebble. Note the presence of a coal fragment (vegetal organic matter) enveloped by a thin calcite halo, as observed for the other rigid elements.

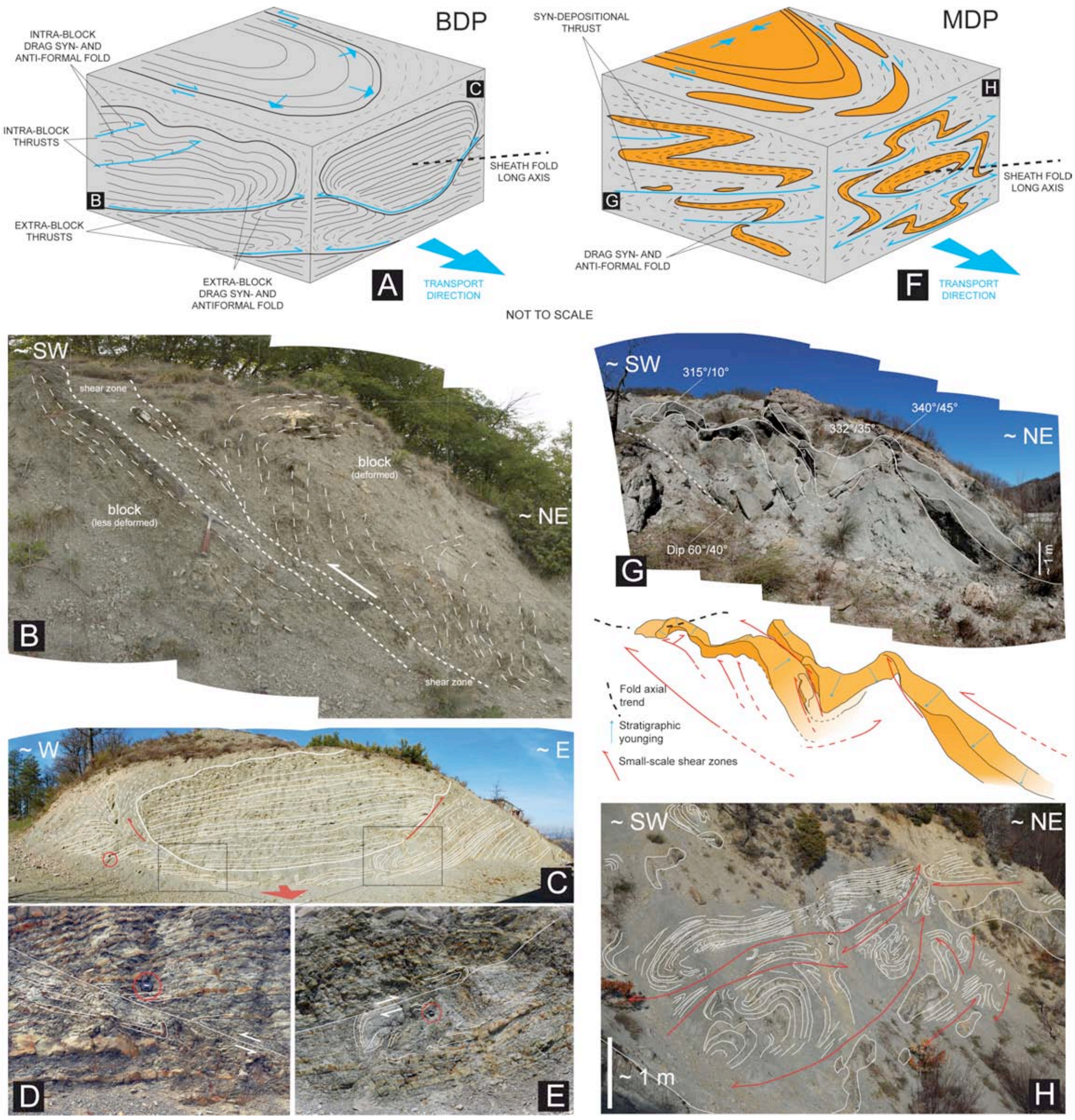

Figure 8: Early Rupelian Specchio MTC (Pessola Valley outlier). A) Conceptual block diagram representing structural associations (inspired from Bradley and Hanson, 1998), which characterize block-dominated portions (BDP). Representative features and relative structural data used for kinematic analysis are indicated. B) Photo-mosaic and line drawing representing a shear zone underlined by a matrix horizon, which separates two block portions (intra-block thrust). This structural association represents the longitudinal side of the block diagram shown in A. Hammer for scale. C) Photo-mosaic and line drawing showing a block overriding another through an intra-block shear

zone. The cut is roughly perpendicular to the main inferred transport direction (transparent red arrow). D) and E) Close-ups showing in detail the same shear surface characterized by two apparent opposite shear senses. This structural association represents the transversal side of the block diagram shown in A. Hammer and Camera lens cap (circled) for scale, 7 cm in diameter. F) Conceptual block diagram representing structural associations (inspired from Bradley and Hanson, 1998), which characterize matrix-dominated portions (MDP). Representative features and relative structural data used for kinematic analysis are indicated. G) Photo-mosaic and interpretation of a meso-scale folding system involving a single thick, coarse-grained sandstone bed, comprised within a MDP (structural data are labeled). Asymmetries and relative vergences are roughly uniform (apart from few minor backthrusts). Note the sheath-like geometry shown by the main fold apex (left side). This structural association represents the longitudinal side of the block diagram shown in F. H) Photo and line drawing of a MDP characterized by complex folding due to the occurrence of several opposite verging shear zones, causing a generalized buckling of structures. This structural association represents the transversal side of the block diagram shown in F.

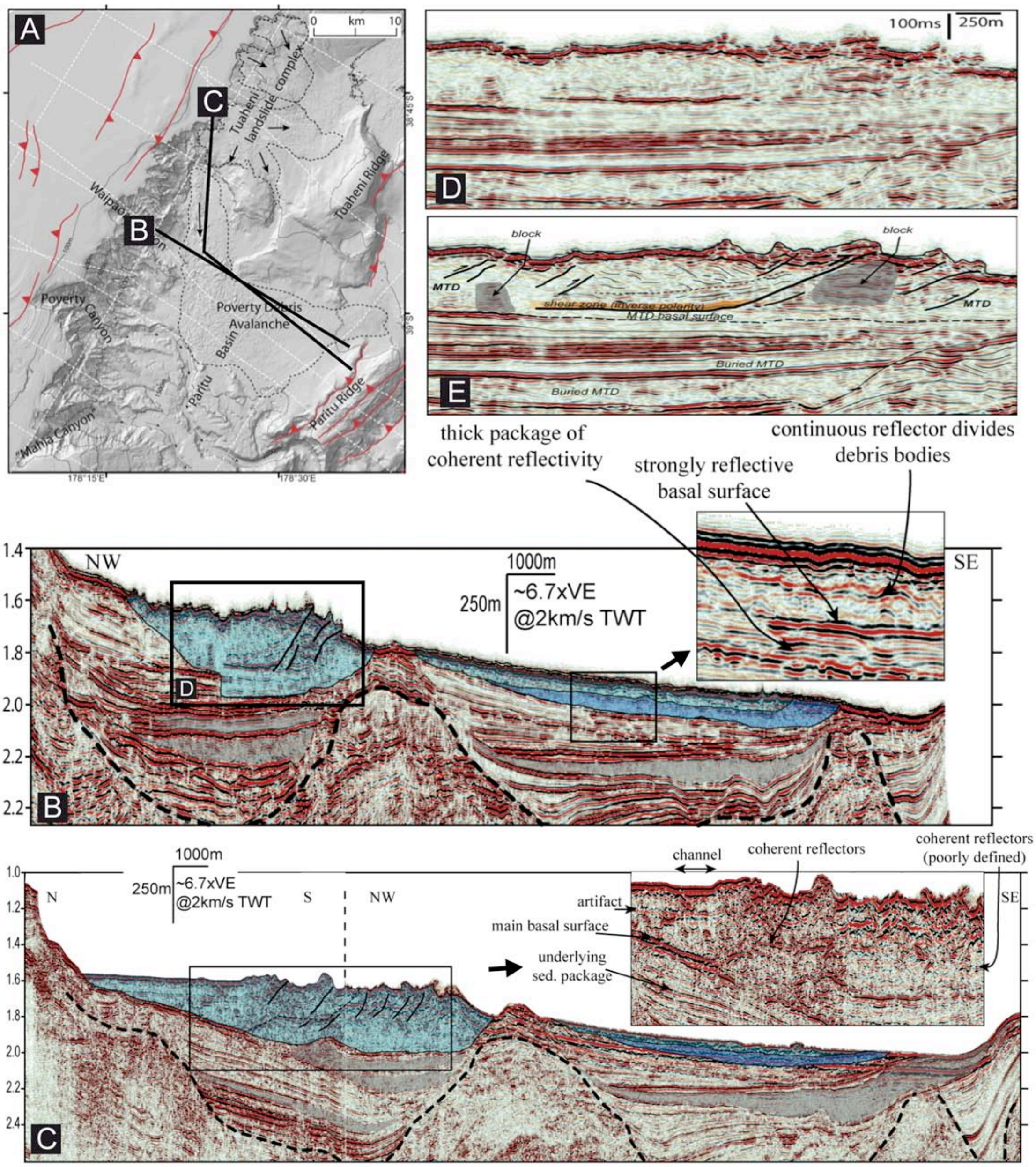

Figure 9: A) Shaded relief map showing the location of the following MCS profiles (B, C and D), extent of the landslide deposits (dotted line) and the interpreted source area. Inferred directions of transport (black arrows) and main thrust fault traces (red toothed lines). B) MCS profile of the Poverty MTC (light and dark blue overlays represent the two main component bodies) showing its internal reflections and the host stratigraphy characterized by buried MTDs (gray overlay). In the inset is represented an enlargement of the MCS profile in the distal part of the MTC, showing the amalgamation between at least two

MTDs (weak continuous reflector) and the basal shear zone (strong discontinuous reflector). C) MCS profile of the Poverty MTC roughly parallel to the line represented in B with inclusion of the most proximal zone and part of the headwall slide scar. The same features observed in B are labeled. The inset represents a close-up of the MCS profile in the proximal part of the MTC characterized by the thickest accumulation and overall compressional regime, as testified by the dominance of thrust faults. D) Slice and E) interpretation of part of the MCS profile of B with indication of the main recognizable features. Note the structurally confined depositional patterns of the sedimentary cover. The weak, discontinuous reflectors characterizing the slide blocks and the strong, coherent reflector representing the main basal shear zone and the flat part of a ramping thrust fault cutting the entire deposit. Modified from Mountjoy and Micallef (2012).

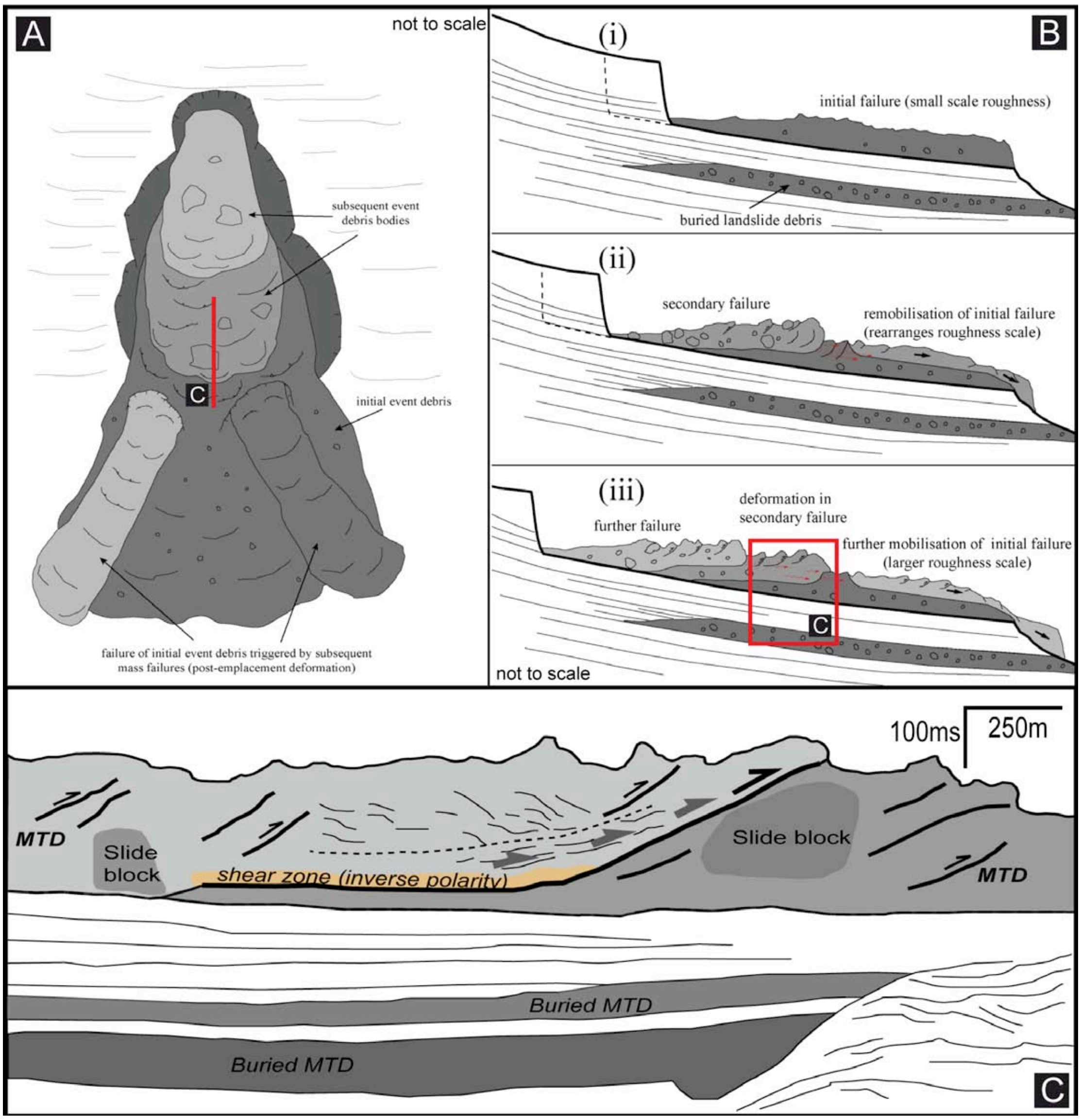

Figure 10: A) Schematic cartoon showing the morphology and the main superficial features of the Poverty MTC in plan view. B) Conceptual scheme showing the three evolutionary stages (from i to iii) of the inferred retrogressive landsliding process, the slide masses' amalgamation and the consequent re-destabilization of the upper, frontal part of the preceding deposit (i.e. "progressive landsliding"). C) Simplified representation of the MCS profile slide of fig. 9D and 9E with identification and interpretation of the main actual structures. To insert the interpreted profile in the proposed framework, the approximate position of the synthetic profile slice has been labeled in A and B.

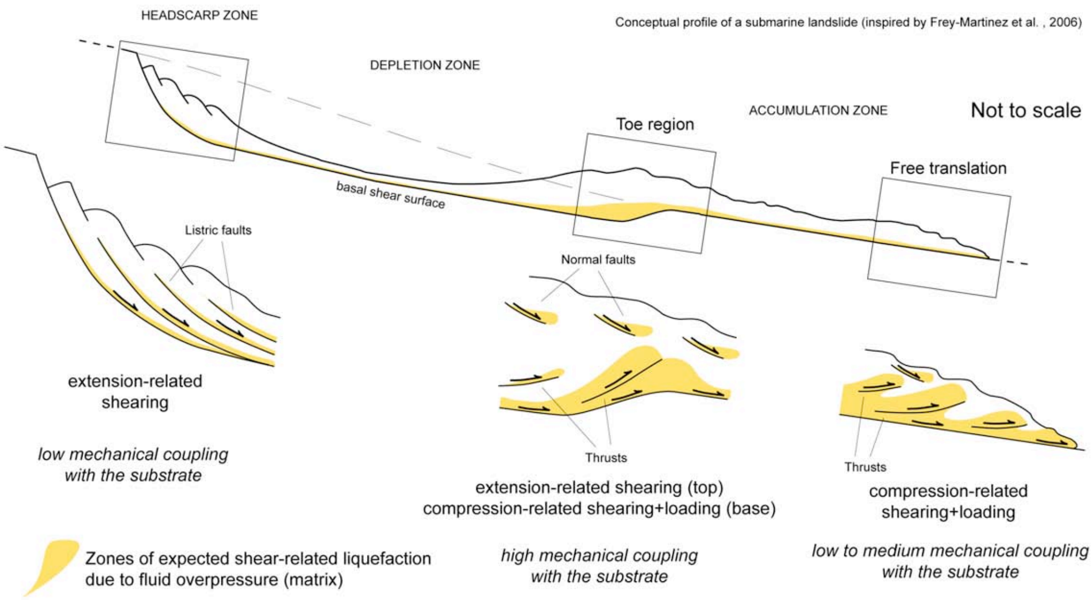

Figure 11: Conceptual profile of a submarine landslide complex with identification of the possible zones where the bulk of mass transport-related deformation occurs and indication of the inferred deformation mechanisms. Relatively thick, matrix-dominated portions and matrix-rich shear zones are thought to represent the products of such localized enhanced progressive deformation (from extensional to compressional, and combination thereof), characterizing specific portions of the MTD which in turn roughly define the three main steps of the slide evolution. Inspired from Frey-Martinez et al. (2006).